Optical electron–hole tweezers in semiconductors

2006 J. Phys.: Condens. Matter 18 729

(http://iopscience.iop.org/0953-8984/18/2/026)

INSTITUTE OF PHYSICS PUBLISHING JOURNAL OF PHYSICS: CONDENSED MATTER

J. Phys.: Condens. Matter **18** (2006) 729–740 doi:10.1088/0953-8984/18/2/026

Optical electron–hole tweezers in semiconductors

R Binder[1] **and M Lindberg**[2]

[1] College of Optical Sciences, University of Arizona, Tucson, AZ 85721, USA
[2] Institutionen för Fysik, Åbo Akademi, Porthansgatan 3, 20500 Åbo, Finland

Received 25 July 2005
Published 16 December 2005
Online at stacks.iop.org/JPhysCM/18/729

Abstract

The theory of transversal light forces on electron–hole pairs in semiconductors has been formulated recently (Lindberg and Binder 2003 *J. Phys.: Condens. Matter* **15** 1119), but only light forces from single Gaussian beams were considered. In the present paper, it is shown theoretically that Hermite–Gaussian beams can be used to reduce and even reverse natural wavepacket spreading. Furthermore, a spatially moving beam can be used to displace and accelerate an electron–hole plasma, in analogy to well-known optical tweezers in atomic systems. The light forces exerted by Hermite–Gaussian beams appear to be robust and therefore of possible practical importance.

1. Introduction

Our previous study of light forces on electron–hole (e–h) pairs in semiconductors [1] can be viewed as part of a general quest of the semiconductor community to identify analogies between optical processes in semiconductors and atoms. Other examples, for which theoretical analysis and experimental verification already exist, include photon echoes, optical Stark shift and Rabi floppings (see, e.g., [2–16] and for a comprehensive review [17]). Such analogies are often useful for the understanding of basic nonlinear optical phenomena in semiconductors. However, there are generally significant differences between nonlinear effects in atoms and semiconductors, because atoms can often be treated very successfully as two-level systems, while the system of electron–hole pairs in semiconductors has to be treated as a many-particle system.

In atomic systems, the transversal light force, originally proposed by Ashkin [18], acts when the atoms are illuminated with an off-resonant light field with a transversal spatial intensity profile. Reviews and text book treatments can be found, for example, in [19–21]. Using this gradient force in combination with moving optical beams, so-called optical tweezers can be created that are able to move objects like atoms, Bose condensates, dielectric spheres or even bacteria [22]. In [23], for example, a gaseous Bose condensate has been transported over distances up to 44 cm. The question naturally arises whether our previous treatment of light forces on e–h pairs can be extended to include optical electron–hole tweezers. In [1], we concluded that (i) a generalization of the gradient force on e–h pairs can be derived on

the basis of the electron–hole transport equations, (ii) the sign of the transversal light force is reversed compared to atoms (i.e. light with frequencies tuned below the interband transition frequencies yields a repulsive force between the light beam and a pre-existing electron–hole plasma), (iii) the use of a single pulse with a Gaussian spatial beam profile can induce only small movements of the e–h plasma, due to the limitations of finite-lifetime effects, natural wavepacket spreading, and the limitation of relatively large (micron-sized) beam waists.

In the following, we revisit the issue of wavepacket spreading and controlled movement of the e–h plasma using the same theory as derived and evaluated in [1]. In contrast to [1], we use a Hermite–Gaussian beam profile. After a brief summary and review of the theoretical framework (section 2), we present numerical solutions for spatially fixed Hermite–Gaussian beams in section 3, and similarly for a moving beam in section 4, and we summarize our results in section 5.

2. Review of the theoretical model

In this section, we briefly review the theory established in [1] and specify the equations used in the numerical evaluations presented below (sections 3, 4).

We use the following Hamiltonian for electrons and holes coupled to an optical field:

$$\begin{aligned}\hat{H} = \hbar\Delta \int \mathrm{d}\vec{r}\, \Psi_{\mathrm{e}}^{\dagger}(\vec{r})\Psi_{\mathrm{e}}(\vec{r}) \\ - \frac{\hbar^2}{2m_{\mathrm{e}}} \int \mathrm{d}\vec{r}\, \Psi_{\mathrm{e}}^{\dagger}(\vec{r})\nabla^2\, \Psi_{\mathrm{e}}(\vec{r}) - \frac{\hbar^2}{2m_{\mathrm{h}}} \int \mathrm{d}\vec{r}\, \Psi_{\mathrm{h}}^{\dagger}(\vec{r})\nabla^2\Psi_{\mathrm{h}}(\vec{r}) \\ - \int \mathrm{d}\vec{r}\, \vec{\mu}\cdot\vec{E}(\vec{r})\Psi_{\mathrm{e}}^{\dagger}(\vec{r})\Psi_{\mathrm{h}}^{\dagger}(\vec{r}) - \int \mathrm{d}\vec{r}\, \vec{\mu}\cdot\vec{E}^{*}(\vec{r})\Psi_{\mathrm{h}}(\vec{r})\Psi_{\mathrm{e}}(\vec{r}). \end{aligned} \tag{1}$$

Here, the electron and hole bands are assumed to be parabolic and characterized by the effective masses m_{e} and m_{h}, and the coupling to the light field is described by a local dipole approximation involving the dipole matrix element $\vec{\mu}$ and the envelope of the light field amplitude $\vec{E}(\vec{r})$. The centre frequency ω_0 of the light pulse is assumed to be detuned from the semiconductor bandgap E_{g} by the amount $\Delta = E_{\mathrm{g}}/\hbar - \omega_0$. The Coulomb interaction between the charge carriers is neglected here, which limits the validity to systems with local charge neutrality (i.e., no space-charge fields) and unbound electron–hole pairs (i.e., no excitons). While neglecting exciton effects may seem like an very restrictive approximation, we point out that the light force discussed below accelerates electrons and holes in the same direction, i.e. it does not effect a significant spatial separation (apart from the slight difference in the values of the forces on and accelerations of electrons and holes). Therefore exciton effects, which require electrons and holes to stay together while being accelerated, would not counteract the light-induced acceleration. We will discuss the expected modifications of our results due to Coulomb effects where appropriate.

The creation ($\Psi^{\dagger}$) and annihilation (Ψ) operators are used to define the Wigner distributions for electrons (W_{e}) and holes (W_{h}),

$$W_{\mathrm{e,h}}(\vec{R},\vec{K}) = \int \mathrm{d}\vec{r}\, \mathrm{e}^{\mathrm{i}\vec{K}\cdot\vec{r}} \langle \Psi_{\mathrm{e,h}}^{\dagger}(\vec{R}+\vec{r}/2)\Psi_{\mathrm{e,h}}(\vec{R}-\vec{r}/2)\rangle \tag{2}$$

as well as that of the interband polarization

$$P(\vec{R},\vec{K}) = \int \mathrm{d}\vec{r}\, \mathrm{e}^{-\mathrm{i}\vec{K}\cdot\vec{r}} \langle \Psi_{\mathrm{h}}(\vec{R}-\vec{r}/2)\Psi_{\mathrm{e}}(\vec{R}+\vec{r}/2)\rangle. \tag{3}$$

Assuming the spatial variation of the light intensity to be sufficiently small, so that we can make a gradient expansion for the field amplitude neglecting all derivatives of order two

or higher, we obtain the following equations of motion:

$$\frac{\partial}{\partial t}\, W_{\mathrm{e,h}}(\vec{R},\vec{K}) = -\frac{\hbar}{m_{\mathrm{e,h}}}\, \vec{K}\cdot\nabla_{\vec{R}}\, W_{\mathrm{e,h}}(\vec{R},\vec{K}) + \mathrm{i}(\vec{\mu}\cdot\vec{E}(\vec{R})\; P^*(\vec{R},\sigma_{\mathrm{e,h}}\,\vec{K}) - \vec{\mu}\cdot\vec{E}^*(\vec{R})\; P(\vec{R},\sigma_{\mathrm{e,h}}\,\vec{K})) - \tfrac{1}{2}\,(\nabla_{\vec{R}}(\vec{\mu}\cdot\vec{E}(\vec{R}))\cdot\;\nabla_{\vec{K}}\; P^*(\vec{R},\sigma_{\mathrm{e,h}}\,\vec{K}) + \nabla_{\vec{R}}(\vec{\mu}\cdot\vec{E}^*(\vec{R}))\cdot\;\nabla_{\vec{K}}\; P(\vec{R},\sigma_{\mathrm{e,h}}\,\vec{K})) \tag{4}$$

where $\sigma_{\mathrm{e}} = +1$ belongs to the electron (index e) and $\sigma_{\mathrm{h}} = -1$ to the hole (index h) equation, and

$$\frac{\partial}{\partial t}\, P(\vec{R},\vec{K}) = (-\mathrm{i}\Delta-\gamma)\; P(\vec{R},\vec{K}) + \mathrm{i}\left(\frac{\hbar}{2m_{\mathrm{e}}}+\frac{\hbar}{2m_{\mathrm{h}}}\right)\left(\frac{1}{4}\nabla^2_{\vec{R}}-\vec{K}^2\right)P(\vec{R},\vec{K}) - \left(\frac{\hbar}{2m_{\mathrm{e}}}-\frac{\hbar}{2m_{\mathrm{h}}}\right)\vec{K}\cdot\nabla_{\vec{R}}\; P(\vec{R},\vec{K}) + \mathrm{i}\vec{\mu}\cdot\vec{E}(\vec{R})(1-W_{\mathrm{e}}(\vec{R},\vec{K})-W_{\mathrm{h}}(\vec{R},-\vec{K})) - \tfrac{1}{2}\nabla_{\vec{R}}(\vec{\mu}\cdot\vec{E}(\vec{R}))\cdot\;\nabla_{\vec{K}}\;(W_{\mathrm{e}}(\vec{R},\vec{K})-W_{\mathrm{h}}(\vec{R},-\vec{K})). \tag{5}$$

We have added a phenomenological dephasing rate γ in the equation to approximate the physical dephasing processes.

In the following section, we present numerical solutions of equations (4) and (5), assuming non-zero initial conditions for electron and hole populations, zero initial conditions for the interband polarization P, and using time-independent (section 3) and time-dependent (section 4) spatial light field profiles. For simplicity, we assume the semiconductor to be one-dimensional.

3. Subnatural spatial widths and spatial compression

In this section we address the question whether an optical pulse can prevent an incoherent e–h plasma, which has initially a finite spatial extension, from spreading, or even can effect spatial compression of the plasma. We recall that, in [1], we have shown that a light pulse with finite spatial extension centred in frequency below the absorption edge (i.e. below the bandgap E_{g} in the case of vanishing Coulomb interaction or below the lowest exciton resonance in the case where exciton effects are important) yields a repulsive force on the plasma. Specifically, we studied the action of a single-peak Gaussian spatial light profile of the form

$$E(X,t) = E(t)G(X,\sigma_x) \tag{6}$$

where

$$G(X,\sigma_x) \equiv \exp\left(-2\ln 2\frac{X^2}{\sigma_x^2}\right). \tag{7}$$

A plasma, initially located, say, to the left of the light field's intensity peak, experiences a light force to the left and also natural wave spreading related to the distribution of momentum states of the plasma. We also found that, given the time constraint that comes from the finite life time of the plasma (the radiative recombination time in direct-gap semiconductors is of the order of nanoseconds), the available forces can only produce very small displacements. The use of an attractive light force could in principle be advantageous, but, in our case, it can be obtained only by tuning the light field above the transition frequencies, i.e. above E_{g}. This

has a practical disadvantage because, ideally, the only effect of the light field is a force on the existing plasma, while in this case it gets strongly absorbed, creating additional e–h plasma as an unwanted side effect.

For these reasons, we study in the following the effects of a light pulse that has a double-peaked spatial structure, and we place an initial e–h plasma between the two peaks of the light intensity. Specifically, we use, as the initial distribution for the e–h plasma, the following Gaussian form in real and momentum space:

$$W_{\mathrm{a}}(X, K, t_0) = W_{\mathrm{a}0} G^2(K, \sigma_k) G^2(X, \sigma_x) \tag{8}$$

with a = e, h. The plasma density has a single peak at $X = 0$ and a momentum spread of order σ_k. The initial polarization is chosen to be zero, because we are simulating an incoherent e–h plasma. For the light field amplitude, we choose a Hermite–Gaussian pulse in space (leading to a double-peaked structure in the intensity) and a temporal shape that contains a switch-on phase, and constant-amplitude phase, and a switch-off phase. Specifically, we choose

$$E(X,t) = E_0 \exp(-\mathrm{i}\omega_0 t) \frac{X - X_0(t)}{\sigma_{\mathrm{H}}} G(X - X_0(t), \sigma_{\mathrm{H}}) \begin{cases} G(t, \sigma_t) & \text{if } t < 0 \\ 1 & \text{if } 0 \leqslant t < \hat{t} \\ G(t - \hat{t}, \sigma_t) & \text{if } \hat{t} \leqslant t. \end{cases} \tag{9}$$

Here, the spatial profile is centred about $X_0(t)$, i.e. the intensity has a double-peaked structure symmetric about $X_0(t)$, and we allow in principle the beam to move in space. However, in this section, we discuss only spatially fixed beams with $X_0(t) = 0$ (i.e. the double-peaked structure is symmetric about $X = 0$). In the next section (section 4), we investigate the action of a moving beam with time-dependent $X_0(t)$.

In the numerical simulation, we choose the following parameter values: $m_{\mathrm{e}} = 0.067 m_0$, $m_{\mathrm{h}} = 0.197 m_0$ (m_0 is the electron mass in vacuum), $\hbar\omega_0 = E_{\mathrm{g}} - 40$ meV, $\mu E_0 = 60$ meV, $\sigma_{\mathrm{H}} = 200 a_0 = 2\ \mu$m, where the Bohr radius a_0 is taken to be 100 Å, $\sigma_t = 2$ ps, $\hat{t} = 2\sigma_t$, $W_{e0} = W_{\mathrm{h}0} = 0.6$, $\sigma_k = 0.5 a_0^{-1}$, $\sigma_x = 100 a_0 = 1\ \mu$m.

In figures 1 and 2 we show the spatial density profiles for electrons and holes at various times before, during and after the pulse. The computational domain in time begins at $t = -6$ ps, and the corresponding initial density profiles (the same for electrons and holes) show a single-peaked structure centred at $X = 0$. The light pulse is then turned on smoothly with a time constant of 2 ps, until it reaches its maximum value at $t = 0$. The intensity is then kept constant until $t = 4$ ps and then switched off with a time constant of 2 ps. We see that at $t = 0$, the density profiles develop a double-peaked structure. This is nothing but the virtual carriers created by the off-resonant light field. Since the light is strongly detuned below the resonance, the virtual carriers live only as long as the light field is turned on. Similar to the well-known case of adiabatic following (see for example [24]), the virtual carrier density follows the pulse intensity, i.e. it remains constant during the time interval of constant light amplitude between 0 and 4 ps. Figures 1 and 2 show that, at $t = 0$, the value of the density at $X = 0$ does not deviate visibly from its initial value. This is expected since the light field is zero at $X = 0$. However, at later times, for example at $t = 4$ ps, the density at the centre ($X = 0$) increases significantly. Moreover, immediately after the pulse is switched off (roughly at $t = 6$ ps), when the virtual carriers are gone, the central peak of the density profile is significantly narrower than the initial density profile. This shows that the light field has successfully prevented the plasma from its natural spreading, possibly even leading to a spatial compression of the electron and hole plasma (we will discuss this point in more detail below). At times greater than 6 ps, the light field is zero and the plasma evolves freely. The electron plasma shows much faster spatial spreading with two outward-moving peaks, while the holes show less spreading and,

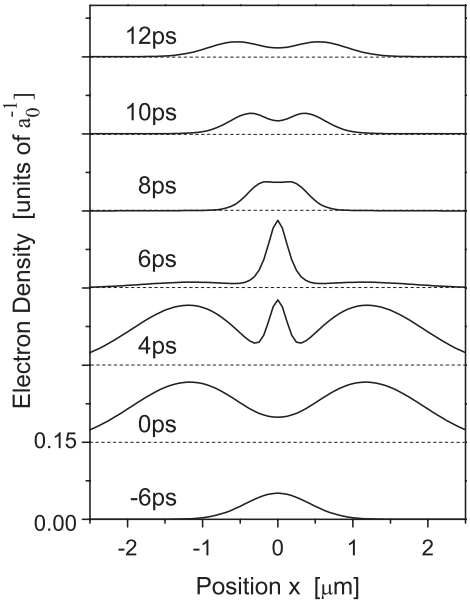

Figure 1. Spatial profile of electron density for different times (from bottom to top): −6, 0, 4, 6, 8, 10 and 12 ps. For all times except −6 ps, the zero line has been shifted for clarity as indicated by the horizontal dashed lines.

instead of two outward-moving peaks, exhibits only small shoulders on either side of the central peak. The following interpretation, which is based on a detailed analysis of the full Wigner functions in real and momentum space, can explain the features seen in the freely evolving plasmas ($t \geqslant 6$ ps). The light field, while present, accelerates the carriers in the following way: carriers at positive x (roughly between $x = 0$ and 1 μm) feel the repulsive force of the light peak centred at about $x = 1$ μm and are accelerated to the left (towards negative x). Correspondingly, the carriers on the left between 0 and -1 μm are accelerated to the right. In the case of the electrons, the force is large enough so that the movements to the right and left lead to the peaks that are clearly visible in figure 1 at $t = 10$ and 12 ps. At these times, the carriers forming the peak at positive x are the ones originating at negative x and vice versa. The same effect holds in principle for the holes as well, but the velocity of the holes is reduced by a factor of m_e/m_h compared to that of the electrons. The reason for the smaller velocity follows immediately from the fact that the forces on electrons and holes are the same (this holds at least in the limiting case of adiabatically eliminated interband polarizations, as shown in [1]). With the force on the holes being the same as that on the electrons, the resulting acceleration of the holes is reduced by the mass factor.

To further analyse and summarize the main features seen in figures 1 and 2, we plot in figure 3 the spatial width of the electron and hole density profiles, defined by

$$\sigma_a(t) = \left[\frac{8 \ln 2}{N_a} \int dX \frac{dK}{2\pi} \left(X - \frac{\langle X_a \rangle}{N_a} \right)^2 W_a(X, K) \right]^{1/2} \tag{10}$$

with

$$\langle X_a \rangle = \int dX \frac{dK}{2\pi} X W_a(X, K) \tag{11}$$

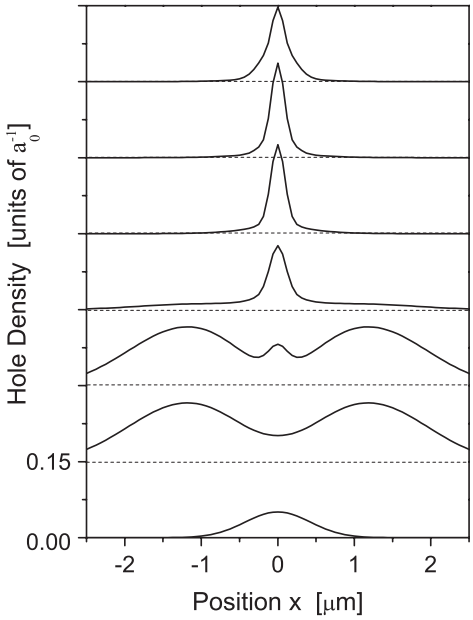

Figure 2. Same as figure 1, but for holes.

and

$$N_{\rm a} = \int {\rm d}X \, \frac{{\rm d}K}{2\pi} W_{\rm a}(X, K). \tag{12}$$

We note that, while the light pulse is on, i.e. roughly from -2 to 6 ps, the width is dominated by the virtual carriers, an effect that is not essential for the present analysis. More important is the fact that, after the pulse is switched off, the width of the density profiles is subnatural. We define a subnatural width as one that is smaller than the width that the density would have required in the absence of any light field. We therefore show in figure 3 the natural width that occurs due to the free evolution of the plasma without any light field, choosing the same initial time (-6 ps) and same initial distributions (equation (8)). Since we have chosen simple Gaussians for the initial conditions, one can obtain an analytical result for the natural spreading, which is

$$\sigma_{\rm a}^{\rm (nat)}(t) = \left[\sigma_x^2 + 2 \ln 2 \sigma_k^2 \left(\frac{\hbar t}{m_{\rm a}} \right)^2 \right]^{1/2}. \tag{13}$$

This is similar to the spreading of a quantum mechanical Gaussian wavepacket, but note that, in contrast to a quantum mechanical Gaussian wavepacket, the initial widths σ_x and σ_k are independent variables within the Wigner function approach used here. Equation (13) shows that, as expected, the heavier particles (in our case the holes) suffer less natural spreading at a given time compared to the lighter particles (the electrons). Figure 3(a) shows that, in a time interval roughly from 6 to 12 ps, the electron spatial width is smaller than the natural width (i.e. subnatural), but not smaller than the initial width (i.e. there is no compression of the density profile). In contrast, the holes (figure 3(b)) show a spatial width that is not only less than the natural width, but also significantly less than the initial width. In other words, the light field has succeeded in actually compressing the spatial profile of the holes. Note that the fast increase of the electron spatial width in this time interval ($t > 6$ ps) is related to the free

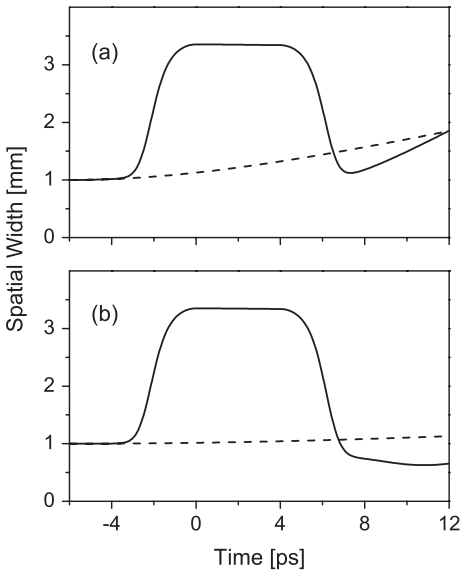

Figure 3. Spatial width of electron (a) and hole (b) density versus time.

evolution of the two peaks (one moving to the right and one to the left), where the velocity of the peaks is governed by the acceleration during the presence of the light pulse and the electron's mass (see figure 1). In other words, the spreading in this situation does not follow the simple form of a spreading Gaussian according to equation (13). As discussed above, the light-induced velocities of the holes are reduced by the mass factor with respect to those of the electrons, which explains the smaller broadening of the hole width at times greater than 6 ps. Indeed, as discussed above, the fact that the holes at positive x are accelerated toward negative x and vice versa, combined with the fact that the induced velocities are quite small, can explain the fact that the minimum spatial width occurs at a time much later than the end of the light pulse (approximately at $t = 10$ ps).

4. Moving action of electron–hole tweezers

In the previous section, we have shown that a light field with a double-peaked intensity pattern exerts a force on an e–h plasma (situated in-between the two light intensity peaks) that can effectively trap the plasma and lead to subnatural spatial widths and even compression. In the following, we study the effect of a double-peaked light pulse moving in space. We want to address the question whether the light beam can drag the e–h plasma with it in space.

For the light amplitude, we assume the Hermite–Gaussian (equation (9)) to move in space at a constant velocity v during the time interval from $t_a = -\sigma_t$ to $t_b = \hat{t} + \sigma_t$ (i.e. basically from the time the pulse gets switched on until it is switched off). At times $t < t_a$, we choose the beam to be centred about the fixed position $x = 0$, i.e. $x_0(t) = 0$. During the time interval $[t_a, t_b]$, we have $x_0(t) = v(t - t_a)$, and at times $t > t_b$ we have $x_0(t) = v(t_b - t_a)$. In the numerical simulation, we use $v = 0.1\ \mu\text{m ps}^{-1}$.

In figure 4 we show the initial spatial profiles of the electrons and holes at time $t = -6$ ps and the final profiles at $t = 12$ ps. Clearly, the plasma has moved along with the light beam by a significant distance. We summarize the movement by showing the centre of the spatial profile, $\langle X_e \rangle$ and $\langle X_h \rangle$, together with the spatial centre of the light beam as a function of

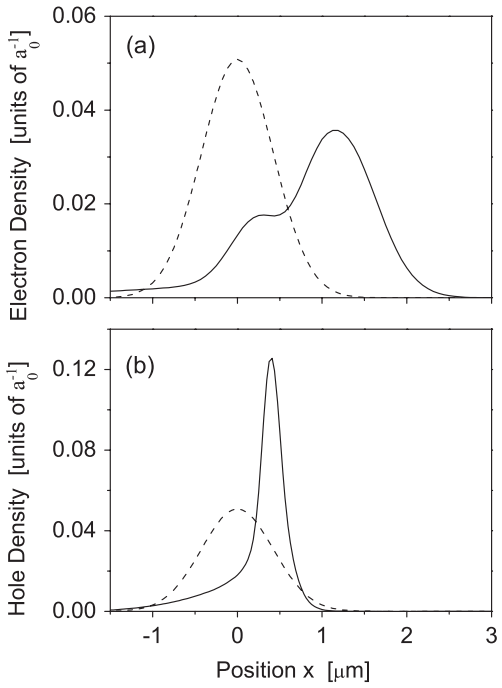

Figure 4. Spatial profile of electron (a) and hole (b) density before the pulse at $t = -6$ ps (dashed lines) and after the pulse at $t = 12$ ps (solid lines).

time in figure 5. The time interval during which the light amplitude is maximum and kept constant (from $t = 0$ to 4 ps) is indicated by the vertical dotted lines. While the light pulse is on, the spatial centres of the electron and hole densities follow almost exactly the position of the beam. This is simply a consequence of the fact that the light creates a large amount of virtual carriers (larger than the initial density). Our simulation shows that the virtual carriers follow the beam at the chosen velocity. A closer inspection of the time dependence of the total (spatially integrated) plasma density (not shown) shows that, at this velocity, the principle of adiabating following (i.e. the fact that the virtual plasma density follows the light intensity) is still preserved. The qualitative behaviour of the spatial widths in the case of a moving beam (shown in figure 6) is similar to that of the stationary beam (see figure 3), but the reduction of the widths of the electron and hole densities is not as large as in the case of a stationary beam.

The fact that the plasma centre-of-mass follows the light field during the times when then virtual plasma dominates over the pre-existing plasma is only of minor importance to our investigation. More important is the fact that, after the light pulse is gone, the spatial centre of the electron and the hole density has shifted to positive x. Moreover, the electron and hole components of the plasma have acquired a certain velocity, which makes them move on after the pulse is gone, i.e. at times larger than about 6 ps. The velocity of the electrons is evidently larger than that of the holes, which is in agreement with the aforementioned mass dependence of the light force and plasma acceleration. We note that, within our model, the motion of the plasma at times after the light pulse has gone is purely ballistic. In a real system, however, incoherent scattering processes lead to friction and diffusion, and the prediction of ballistic motion is certainly invalid on a timescale comparable to or larger than the relaxation time (which depends on the details of the system). Hence, we expect that the observable effect of

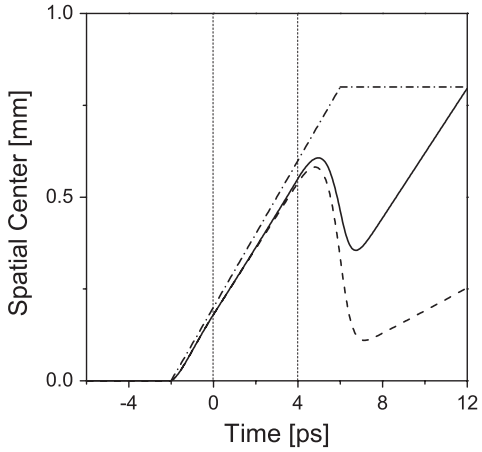

Figure 5. Spatial centre of electron (solid line) and hole (dashed line) versus time. Also shown is the spatial centre of the light field (dash–dotted line). The vertical dotted lines indicate the time interval in which the light amplitude is kept constant.

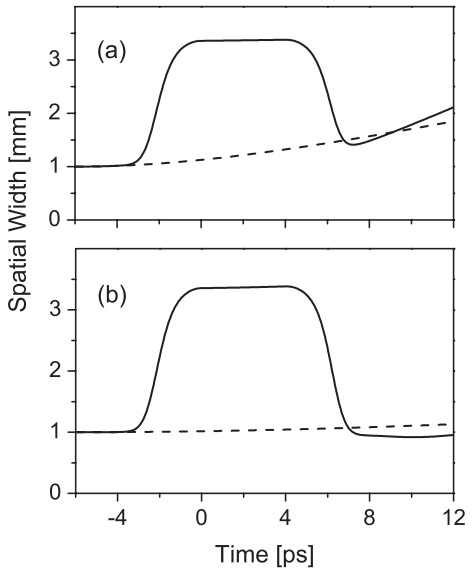

Figure 6. Spatial width of electron (a) and hole (b) density versus time.

light-induced acceleration indicated in figure 5 will generally be smaller than predicted in our idealized treatment.

From figure 5 we see that immediately after the pulse (at about $t = 7$ ps), the electrons have moved by about 0.4 μm. Given the fact that, during the time when the light intensity is kept constant (i.e. between 0 and 4 ps) the light moves exactly 0.4 μm, we can say that the moving light beam acts in a way similar to optical tweezers. It apparently traps the electron plasma and carries it in the potential energy minimum provided by the light. The same effect exists in principle also for the hole plasma, but apparently the displacement of the hole plasma after the pulse is much less than that of the electron plasma. To understand this, we analyse the

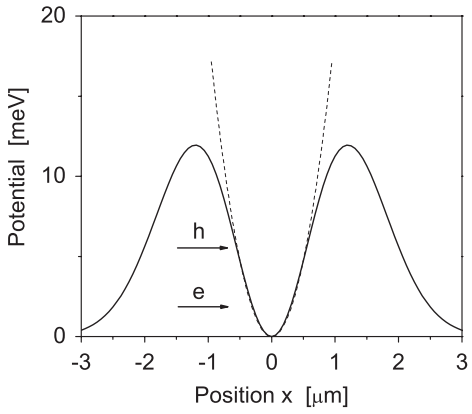

Figure 7. Effective e–h trapping potential $U(x)$ (solid line). Also shown is a harmonic approximation (dashed line) and the maximum amplitudes in a classical model for electrons and hole (arrows); see text for details.

spatial density profiles after the pulse shown in figure 4. We first note that even the electron plasma does not exhibit a perfect displacement. It exhibits a primary density peak centred roughly at $x = 12\ \mu$m and a secondary peak (or shoulder) at the position of the initial density profile. The displacement of the primary peak to the position of $x = 12\ \mu$m is consistent with the ramping velocity of $v = 0.1\ \mu\text{m ps}^{-1}$ and the time instant of 12 ps. The existence of the secondary peak indicates that not all of the carriers get accelerated by the light in the same way. Apparently, this effect of carriers being left behind is even stronger for the holes.

In order to have a simple interpretation of this effect, we analyse the effective trapping potential and provide a simple semi-classical model for the acceleration process. As shown in [1], an approximate expression for the force on the carriers can be obtained within the adiabatic elimination of the optical polarization function. In the limit of zero momentum and vanishing dephasing we have

$$\vec{F}(\vec{R}) = -\nabla_{\vec{R}} \frac{|\vec{\mu} \cdot \vec{E}(\vec{R})|^2}{\Delta}. \tag{14}$$

We note that this expression does not depend on the pre-existing carrier density, and that, for a certain desired force and given detuning, it gives a criterion for the light intensity that is needed. In turn, the light intensity determines the amount of virtual carriers (present only during the duration of the light pulse). Hence, within this model, the densities of the pre-existing carriers and the virtual carriers are independent of each other.

Within the one-dimensional model that we use in our calculations, the force corresponds to a potential energy profile of

$$U(X) = \frac{|\mu E(X)|^2}{\Delta}. \tag{15}$$

We show this potential in figure 7, along with a parabolic approximation valid at small x. Clearly, the actual potential has a finite barrier height of about 12 meV in our case. If we assume, for the sake of argument, a classical particle with mass m with zero velocity to be at the bottom of the parabolic potential at time $t = 0$, and we furthermore assume the parabolic potential to start moving with velocity v at that time, i.e. for $t > 0$,

$$U(X) = \tfrac{1}{2} m (X - vt)^2 \Omega^2 \tag{16}$$

where Ω characterizes the harmonic potential, the solution of Newton's equation is

$$X(t) - vt = -\frac{v}{\Omega}\sin(\Omega t). \tag{17}$$

Due to the sudden movement of the parabolic potential, the particle acquires an amplitude inside the potential of $A = v/\Omega$, corresponding to a maximum potential energy of $(1/2)mA^2\Omega^2 = (1/2)mv^2$. The potential $U(x)$ in figure 7 is the same for electrons and holes, i.e. independent of the mass m, therefore $m_e\Omega_e^2 = m_h\Omega_h^2$. Consequently, the frequency Ω is larger for electrons than for holes and the amplitude A is smaller for electrons than for holes. The amplitudes are indicated by horizontal arrows in figure 7. Since the real potential has a finite height, it is clear that the heavier particles are more at risk of rolling over the left potential maximum when the potential starts moving to the right. It is simply the inertia of the particles that makes heavier particles more difficult to accelerate than light particles, and this is the basic reason for the optical tweezers action shown in figures 4 and 5 to be more effective for electrons than for holes. The inertia-related leakage of particles out of the trapping potential can, in principle, be minimized through a careful choice of light-beam acceleration and optimized light intensity, but such detailed considerations are beyond the scope of this work.

We finally note that the light-induced spatial separation of electrons and holes will be significantly reduced if not cancelled by the Coulomb interaction. It is well known that the internal electric field (space-charge field) tends to minimize the distance between electrons and holes and make their respective velocities equal. In the ballistic regime, this leads to ambipolar drift, while in the diffusive regime it leads to ambipolar diffusion. The timescale on which the internal space-charge field removes a local charge imbalance is called the dielectric relaxation time, and in electron–hole systems this is usually in the sub-picosecond regime (see, for example, p 180 of [25]). While our simplified model does not include Coulomb effects, it is physically reasonable to assume that the displacements one would obtain from a calculation with Coulomb effects are probably almost the same for electrons and holes (and may be close to the average of the electron and hole displacements found in our simplified model).

5. Summary

We have analysed the action of a double-peaked light intensity profile on a non-interacting electron–hole plasma. The numerical solutions of the transport equations for the Wigner functions of electrons, holes, and interband polarization revealed that a spatially fixed Hermite–Gaussian light pulse can prevent the natural spatial spreading of the plasma and even lead to spatial compression. The underlying transversal light force has been discussed in [1], but the application of a Hermite–Gaussian pulse exhibits a much more robust effect on the electron–hole plasma than the one found for a single-peaked Gaussian beam studied in [1]. Furthermore, we have shown above that the robustness of the light force in this configuration also allows for the plasma to be moved in a moving light intensity profile (optical tweezers). Deviations from an ideal tweezers action can be understood in terms of the inertia of the particles and has been found to be strongly dependent on the effective masses of the particles. This kind of optical tweezers for electrons and holes could point the way towards a controlled spatial manipulation of electrons and holes, which could be useful in the context of basic research (e.g. the quest for Bose condensation of excitons) and information technology.

Acknowledgments

This work is supported by Magnus Ehrnrooths Stiftelse, JSOP and COEDIP.

References

[1] Lindberg M and Binder R 2003 *J. Phys.: Condens. Matter* **15** 1119
[2] Mysyrowicz A, Hulin D, Antonetti A, Migus A, Masselink W T and Morkoc H 1986 *Phys. Rev. Lett.* **56** 2748
[3] von Lehmen A, Chemla D S, Zucker G E and Heritage J P 1986 *Opt. Lett.* **11** 609
[4] Fluegel B, Peyghambarian N, Lindberg M, Koch S W, Joffre M, Hulin D, Migus A and Antonetti A 1987 *Phys. Rev. Lett.* **59** 2588
[5] Becker P C, Fragnito H L, Brito Cruz C H, Fork R L, Cunningham J E, Henry J E and Shank C V 1988 *Phys. Rev. Lett.* **61** 1647
[6] Chemla D S, Know W H, Miller D A B, Schmitt-Rink S, Stark J B and Zimmermann R 1989 *J. Lumin.* **44** 233
[7] Hulin D and Joffre M 1990 *Phys. Rev. Lett.* **65** 3425
[8] Webb M D, Cundiff S T and Steel D G 1991 *Phys. Rev. Lett.* **66** 934
[9] Cundiff S T, Knorr A, Feldmann J, Koch S W, Göbel E O and Nickle H 1994 *Phys. Rev. Lett.* **73** 1178
[10] Schneider H and Ploog K 1994 *Phys. Rev.* B **49** 17050
[11] Saiki T, Kuwata-Gonokami M, Matsustue T and Sakaki H 1994 *Phys. Rev.* B **49** 7817
[12] Fürst C, Leitenstorfer A, Nutsch A, Tränkle G and Zrenner Z 1997 *Phys. Status Solidi* b **204** 20
[13] Giessen H, Knorr A, Haas S, Koch S W, Linden S, Kuhl J, Hetterich M, Gruen M and Klingshirn C 1998 *Phys. Rev. Lett.* **81** 4260
[14] Schülzgen A, Binder R, Donovan M, Lindberg M, Wundke K, Gibbs H, Kithrova G and Peyghambarian N 1999 *Phys. Rev. Lett.* **82** 2346
[15] Sieh C, Meier T, Jahnke F, Knorr A, Koch S W, Brick P, Hübner M, Ell C, Prineas J, Khitrova G and Gibbs H M 1999 *Phys. Rev. Lett.* **82** 3112
[16] Nielsen N C, Höner zur Siederdissen T, Kuhl J, Schaarschmidt M, Förstner J, Knorr A and Giessen H 2005 *Phys. Rev. Lett.* **94** 057406
[17] Shah J 1996 *Ultrafast Spectroscopy of Semiconductors and Semiconductor Nanostructures* (*Springer Series in Solid-State Sciences* vol 115) (Berlin: Springer)
[18] Ashkin A 1970 *Phys. Rev. Lett.* **25** 156
[19] Kasantsev A P, Surdutovich G I and Yakovlev V P 1990 *Mechanical Action of Light on Atoms* (Singapore: World Scientific)
[20] Cohen-Tannoudji C 1992 *Fundamental Systems in Quantum Optics (Les Houches, Session LIII)* ed J Dalibard, J M Raimond and J Zinn-Justin (Amsterdam: Elsevier)
[21] Meystre P 2001 *Atomic Optics* (New York: Springer)
[22] Ashkin A and Dziedzic J M 1987 *Science* **237** 1517
[23] Gustavson T L, Chikkatur A P, Leanhardt A E, Gölitz A, Gupta S, Pritchard D E and Ketterle W 2002 *Phys. Rev. Lett.* **88** 020401
[24] Allen L and Eberly J H 1975 *Optical Resonance and Two-Level Atoms* (New York: Dover)
[25] Sapoval B and Hermann C 1995 *Physics of Semiconductors* (New York: Springer)